Letter

Spherical thermal counterflow of superfluid ^{4}He

F. Novotný, Y. Huang, J. Kvorka, Š Midlik, D. Schmoranzer, Z. Xie, and L. Skrbek
Charles University, Faculty of Mathematics and Physics, Ke Karlovu 3, 121 16 Prague, Czech Republic

(Received 20 February 2023; accepted 21 December 2023; published 28 February 2024)

We generate quantum turbulence in *spherically symmetric* thermal counterflow of superfluid ^{4}He driven by a central heater and probe it by second sound attenuation. We show that normal fluid turbulence forms above a certain critical threshold and, in the absence of shear flow, draws energy from a preexisting random tangle of quantized vortices corresponding to Vinen-type turbulence. This experiment can serve as a model flow for cosmological phenomena relating cosmic strings to quantized vortices, for processes occurring in neutron stars, or cosmological structure formation within superfluid models of dark matter.

DOI: 10.1103/PhysRevFluids.9.L022601

Matter flows occurring in Nature on geophysical or astrophysical scales often defy any experimental approach due to their complexity or the sheer length scales involved; a large part of these flows are characterized by a spherical symmetry. Due to its unique properties, cryogenic helium may be used with advantage to provide experimental evidence under conditions exceedingly difficult to attain with classical fluids. Thermally driven flows such as Rayleigh-Bénard convection may be studied in cryogenic helium gas [1], and a much wider range of flows becomes accessible using the superfluid ^{4}He phase (He II), via suitably constructed analogies.

Thermal counterflow (CF) of He II is unique in that it transports heat convectively with local as well as global zero net mass flow. Realized in channels of constant cross section, it belongs to the most investigated quantum flows [2–6]. Here we show that spherically symmetric thermal CF, which so far has attracted only limited attention [5,7,8], displays important features which are in striking contrast with properties of channel CF. Our preliminary data on the decay of spherical CF turbulence in a 3D-printed plastic cell show features of Vinen-type turbulence (see Fig. 2 in Ref. [5]), and this work provides a systematic study revealing unexpected features of this turbulent flow driven in the absence of shear forces. There is no direct classical counterpart of spherical CF. However, for spherically symmetric heat flows the closest analog is buoyancy-driven thermal convection in a gravitational field, occurring typically in the interior of Sun-like stars [9], neutron stars [10,11], or Earth-type planets [12]. From a broader view, condensed matter analogies to cosmological phenomena [13], such as the Kibble-Zurek mechanism [14,15] relating cosmic strings to quantized vortices in superfluids, or the possibility of structure formation in the Universe via the collapse of spherical overdensities within the framework of superfluid models of dark matter [16], make spherical CF interesting to a wide spectrum of scientific communities.

In this work spherical CF is studied above 1 K, where He II displays the two-fluid behavior. Here channel CF can be easily set by applying heat flux $\dot{q}$ to the dead end of a channel with its other side open to the bath of He II; $\dot{q}$ is carried in a convective manner by the normal fluid of density ρ_n. By conservation of mass, a superfluid current arises in the opposite direction and counterflow velocity is established [2–6]: $u_{ns} = \dot{q}/\rho_s sT$, where T is the temperature and s stands for the specific entropy of He II. The motion of the inviscid superfluid component of density ρ_s is constrained. Rotary flow may exist in it only due to quantized vortices, topological line defects, each carrying one quantum of circulation $\kappa = h/m_4 \approx 9.97 \times 10^{-8}\,\mathrm{m^2\,s^{-1}}$, where h is Planck's constant and m_4 is the mass of a ^{4}He atom [17]. For small enough $\dot{q}$ the flow of the viscous normal fluid is laminar, and there are nearly no quantized vortices in the superfluid component [18]. Upon

increasing $\dot{q}$, channel CF becomes turbulent, and a tangle of quantized vortices is generated by extrinsic nucleation and reconnections. The first detailed investigation of channel CF turbulence was performed by Vinen [6]. He introduced a phenomenological model describing a homogeneous random vortex tangle characterized by the vortex line density (VLD), denoted by L. This type of quantum turbulence (QT) is now called *Vinen QT*. Its turbulent spectral energy density peaks at length scales $\ell \approx 1/\sqrt{L}$, where it is driven via the interaction of individual quantized vortices [20]; here ℓ is the mean distance between vortex lines, also referred to as the quantum length scale [5]. The temporal decay of VLD obeys the prediction of the Vinen equation [6] with $L \propto t^{-1}$ at long times. This is contrary to *Kolmogorov QT*, where the energy spectrum contains a classical inertial range of scales characterized, neglecting intermittency corrections, by the famous roll-off exponent $-5/3$. This type of QT, driven at large energy containing scale $M \gg \ell$, displays quasiclassical decay of VLD $L \propto t^{-3/2}$ at long times [5,21].

A natural question and motivation for our work emerges: does spherical CF of He II represent Vinen- or Kolmogorov-type QT? A closer look at channel CF turbulence shows that this flow is indeed complex. Above a first critical velocity $u_{\mathrm{ns}}^{\mathrm{cr1}}$ a vortex tangle is created in the superfluid while the normal fluid remains laminar (so called T I state [2]); its velocity profile is altered by mutual friction [22,23] with details still under investigation. The superfluid velocity profile in a wide channel is almost uniform far from the boundary, and the turbulence in the superfluid component is of the Vinen kind. The temporal decay of VLD originating from the T I state obeys the prediction of the Vinen equation $L \propto 1/t$ [6], as was recently verified experimentally [24,25]. Upon reaching a second critical velocity $u_{\mathrm{ns}}^{\mathrm{cr2}}$ the turbulence appears stronger (the so-called T II state [2]). As suggested theoretically [26] and confirmed by flow visualization [27], this transition marks the onset of turbulence in the normal fluid. The existence of large eddies in the normal fluid subsequently causes, via mutual friction, the creation of large superfluid eddies, and He II enters into a remarkable double turbulent regime in which the large-scale normal and superfluid velocity fields move in opposite directions. In the steady T II state, there are two energy inputs to the superfluid component. Besides the already discussed one at ℓ creating a peak at small scales, there is now a classical-like energy input at large scale mediated by mutual friction. Upon stopping the heat input, the energy peak at ℓ quickly decays, and the energy content at large scales gradually cascades down, forming an inertial range that acquires a classical Kolmogorov form. It results in late classical-like decay of the form $L \propto t^{-3/2}$ [24,25].

Below we show that these basic features of channel CF are in striking contrast with properties of spherical CF. Lacking the channel walls, it represents an unbounded flow, similarly as in 2D studies of cylindrically symmetric flows [28,29]. From these works it is known that a radial temperature gradient must exist in order for a stable steady-state flow to form. Details of the radial temperature gradient are given in the Supplemental Material (SM) [30], following the studies of spherical CF by Varga [7] and by Inui and Tsubota [8], as well as our measurements in channel and spherical CF [31,32]. In this work we generate spherical CF by a tiny 150 Ω resistor (covered by Stycast 2850 epoxy ≈1.8 mm in diameter) located in the center of a spherical cavity of diameter 20 mm made of three brass pieces. Another such heater is placed in the helium bath, allowing one to switch the applied power $\dot{q}$ between the bath and the cell, which is essential for temperature stabilization. QT is probed by second sound attenuation [33]: a pair of circular second sound sensors is placed at the poles of the spherical cavity, causing a small deviation ≈0.5 mm from spherical symmetry. Careful mapping of second sound resonances reveals that below 10 kHz more than 100 standing wave modes can be found. Their identification and calculation of spatial profiles is discussed in the SM [30]. For the measurements we have chosen two modes, at 2950 Hz and 8923 Hz at 1.65 K on account of their isolated frequencies and high Q factors >1000. Their sensitivity profiles are shown in Fig. 1. A Ge/GaAs thermometer is installed on the outer wall of the cell and used to determine the temperature inside and to evaluate helium properties.

In order to drive spherical CF, we apply power $\dot{q}$ ranging up to 200 mW to the spherical heater at different bath temperatures. We perform the steady-state measurements in two ways: (1) by collecting full frequency sweeps across the studied peak at fixed $\dot{q}$ and (2) by continuous tracking

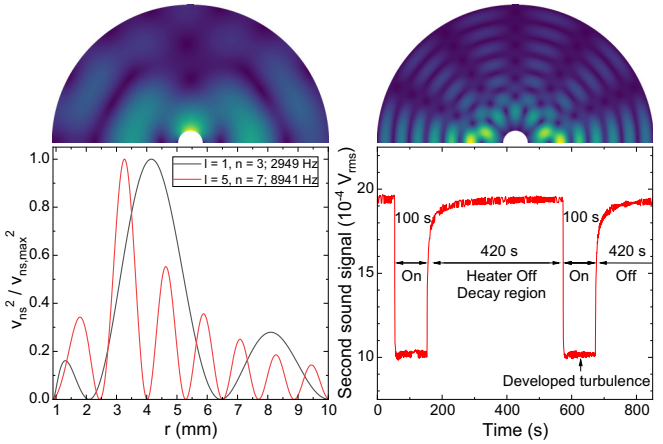

FIG. 1. Top: Spatial sensitivity maps of the resonant modes used, shown in the r-θ half-plane with the z axis oriented normally, expressed in terms of the amplitude squared. Bottom left: Radial amplitude profiles of the second sound resonances integrated over the angle θ. Bottom right: Example of the decay measurement sequence ($T = 1.65$ K, $\dot{q} = 100$ mW).

of the resonance maximum using a PID algorithm while $\dot{q}$ is ramped. In this case the signals are corrected with respect to a linear background and time-averaged. Both methods show good agreement; see Fig. 2. Decay measurements use the tracking algorithm with the results averaged over 50 decays.

As both the VLD distribution, $L(\mathbf{r})$, and the sensitivity profile of the second sound resonance are functions of position in spherical CF, we characterize the steady-state VLD by the excess damping of the second sound resonance, expressed as an inverse quality factor due to quantized vortices, Q_L^{-1}. It can be shown that this damping is proportional to the average VLD weighted by the sensitivity map of the given second sound mode. For an order of magnitude estimate of the overall VLD in the cell, one may also introduce a characteristic VLD, evaluated under the assumption of homogeneity and isotropy: $L^* = 6\pi\,\Delta f(a_0/a - 1)/(B\kappa)$, where a_0 and a are amplitudes of the second sound

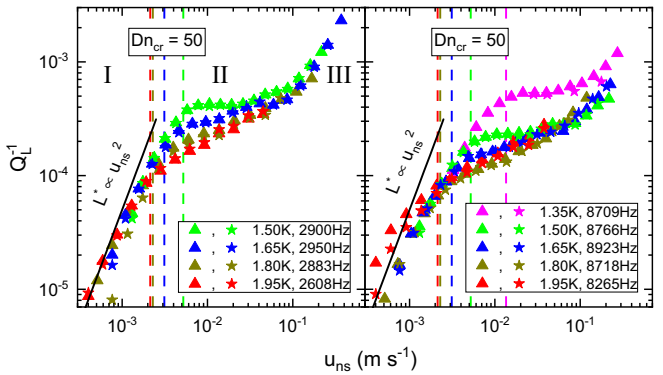

FIG. 2. The damping of second sound resonances due to quantized vortices given in terms of the inverse quality factor Q^{-1} plotted against u_{ns} near the heater surface, measured at the lower (left) and higher second sound resonance (right) at the bath temperatures indicated. Three distinct regimes are observed. Stars (triangles) represent full frequency sweeps (tracker) data; color-coded vertical dashed lines for individual temperature series mark the u_{ns} values for which $Dn_c = 50$, coinciding with the onset of the plateau.

resonance without and with quantized vortices, respectively, B is the mutual friction parameter tabulated in [34] and Δf stands for the full width of the unattenuated second sound resonance [33].

In channel CF, $u_{\rm ns}$ is related to the observed VLD: $L = \gamma^2(u_{\rm ns} - u_{\rm c})^2 \approx \gamma^2 u_{\rm ns}^2$, where $u_{\rm c}$ is the critical velocity typically of order 1 mm/s and γ is a temperature dependent parameter, known with the accuracy of about 20%. In spherical CF, the steady-state profile of local VLD is inhomogeneous: we would expect roughly $L \propto r^{-4}$, since $u_{\rm ns} \propto r^{-2}$. This approach, however, takes into account neither the specific dynamics of vortices in the counterflow, nor the generation and decay of vortices on the surface of the heater, which requires deeper analysis as discussed by Holm [35]. From numerical simulations [8] a vortex shell forms in the vicinity of the heater with maximum density in some nonzero distance from the surface. Finally, $u_{\rm ns}$ is affected by the temperature profile, and we can expect a deviation from $L \propto r^{-4}$; for further details see SM [30].

Figure 2 displays values of Q_L^{-1} vs $u_{\rm ns}$ evaluated at the heater surface. The data sets show that the expected quadratic relationship $Q_L^{-1} \propto L^* \approx \gamma^2 u_{\rm ns}^2$ generally does not hold in the entire range of counterflow velocities, but remains valid for low $u_{\rm ns}$ (regime I), while at high $u_{\rm ns}$ the data seem to agree better with a linear relationship (regime III). We have attempted to detect a critical counterflow velocity at which the vortex tangle is first created; however, as seen from Fig. 2, our sensitivity allows one only to set an upper limit for it, about 1 mm/s. It is a striking observation that for intermediate $u_{\rm ns}$ the observed growth of Q_L^{-1} is much weaker or, in some cases, suppressed (regime II). This region is also the only one showing a systematic temperature dependence, with the plateau-like feature starting first at higher temperatures, while at lower temperatures it happens at higher $u_{\rm ns}$ and more abruptly. In the following we will discuss the origin of this unexpected plateau.

The lower second sound resonance experiences higher damping at any temperature than the higher mode; spatial distribution of VLD may thus be important. We showed [36] that measurements with given harmonic modes give the mode-shape weighted average of VLD in the probed volume. Assuming spherical symmetry $L(r) = \gamma^2 u_{\rm ns}^2 = Ar^{-4}$ and linear damping, we obtain

$$Q^{-1} \propto \frac{\int L(r)\phi^2(r)\, d^3\vec{r}}{\int \phi^2(r)\, d^3\vec{r}} \propto \frac{A\int_{R1}^{R2} \phi^2(r) r^{-2}\, dr}{\int_{R1}^{R2} \phi^2(r) r^2\, dr} \propto u_{\rm ns}^2, \tag{1}$$

where $\phi(r)$ is the radial amplitude profile of the second sound resonance (see Fig. 1) and the integrals are evaluated over the spherical cavity. The obtained scaling $Q^{-1} \propto u_{\rm ns}^2$ means that, under these simplifying assumptions, the experimentally observed plateau in regime II cannot be caused by the interplay of the radial profile of the second sound resonance with the changing spatial distribution of $L(r)$. In reality $L(r) \propto r^{-4}$ is not satisfied exactly due to temperature gradients, especially close to the heater, but we show in the SM [30] that the temperature variations amount to units of mK at most and cannot cause this effect. While perfect spherical symmetry assumed above need not be satisfied in the experiment, this is also unlikely to cause the systematically observed plateau.

It is then natural to ask: Could turbulence in the normal fluid affect the quantized vortices in the superfluid component? Could it be responsible for the slowly growing region at intermediate counterflow velocities? If this were true, the instability in the steady flow of the normal component would have to be triggered at a certain value of the Donnelly number, ${\rm Dn}(r) = u_{\rm n} r \rho_{\rm n}/\eta$, acting as an effective Reynolds number, Re, for the normal fluid of kinematic viscosity $\eta/\rho_{\rm n}$ [5,37]. Furthermore, the critical ${\rm Dn_c}$ would have to be comparable to ${\rm Re_c}$ obtained in a class of classical flows, where some degree of similarity to our case can be claimed. Figure 2 shows the tentative onset of this instability at several temperatures, where the normal fluid fraction changes between $\approx 50\%$ at 1.95 K and $\approx 5\%$ at 1.35 K. This onset agrees quite well with ${\rm Dn_c} \simeq 50$, evaluated at the heater surface, although the first instability may actually occur at a lower Dn before we detect it reliably. The classical instability in diverging channels [38] or in diverging jets [39,40] occurs at reported $20 \lesssim {\rm Re_c} \lesssim 50$, similar to our ${\rm Dn_c}$.

Let us consider why the transition to turbulence in the normal fluid could reduce the number of quantized vortices in the spherical cell, in contrast to channel CF. In channel CF, the shear flow near the walls drives the normal turbulence at large scales, leading to energy transfer via mutual friction to the superfluid, where no large-scale flow would exist otherwise. The cascade process then leads to transfer of energy to smaller scales in both fluids and to generation of additional VLD. On the other hand, in the spherical geometry the flow exhibits essentially zero shear stresses (except near the thin capillary holding the heater), and large vortical structures are thus unlikely to form. The only dynamically relevant length scale is the radius, r. Rotating vortical structures are unlikely to develop around a symmetric central source, although it might, in principle, happen due to imperfections of the cell. More likely, the instability appears in the form of bifurcations as in classical diverging pipe flows, which would mean driving the turbulence at smaller length scales. These perturbations would at first draw energy from small-scale fluctuations in the superfluid velocity field via the mutual friction force acting between randomly moving quantized vortices and the normal flow, hence it seems plausible that the normal fluid turbulence is triggered and partly driven by its preexisting superfluid counterpart at the onset, before sufficient energy input due to imperfect symmetry is provided that would warrant the development of large flow structures.

We propose the following model of QT in our cell. At the lowest u_{ns}, energy is mainly imposed into the excitation of quantized vortices, while the effect of the laminar normal flow is negligible. For u_{ns} between $\approx$2 mm/s and $\approx$100 mm/s, the energy of the vortex tangle is additionally consumed by the emergence of turbulence in the normal component, driven at small scales by the superfluid and limited at first to the vicinity of the heater. This leads to a lower energy budget for the tangle itself and results in a slower growth rate, as observed. The energy transfer must occur at small scales of order ℓ as there is no efficient way to drive normal turbulence at larger scales. For this reason, the energy transfer from normal to superfluid component observed in channel CF is absent in the spherical case. Finally, for u_{ns} higher than $\approx$100 mm/s, the direct energy input of the heater may become divided between the classical and superfluid turbulence, the imperfections of the cell now driving the instability in the normal flow with sufficient intensity. Upon increasing $\dot{q}$, the normal turbulence may thus develop large-scale eddies and spread into the entire cell. At the same time, small eddies of size $\approx \ell$ will receive energy from large-scale flow and can in turn excite additional quantized vortices, as observed. This scenario is confirmed by measurements of the temporal decay of $L^*(t)$, according to the protocol shown in Fig. 1. Power $\dot{q}$ is applied to the heater in the cell for $\approx$100 s, resulting in the development of statistically steady QT. Then $\dot{q}$ is switched from the heater in the cell to an identical heater in the He bath and QT decays. This is repeated $\approx$50 times and averaged. In order to obtain the correct power law of the decay, one has to take into account the virtual origin time t_0 and remnant vortex line density L_0^* remaining in the cell after individual decays.

Figure 3 displays almost two decades of inverse time decay of $L^*(t)$, a fingerprint of the Vinen-type QT [5]. We point out that the decay data were taken mostly at lower velocities in the first two regimes of turbulence described above, with the single exception of the data series at 1.65 K and 0.127 m/s, which corresponds to the end of the plateau in Fig. 2. The reason is difficulty in stabilizing the frequency of the second sound resonance used for detection of vortices, which is strongly temperature-dependent. It is thus possible that a quasiclassical decay with $L^*(t) \propto t^{-3/2}$ could be observed at higher initial velocities above the plateau, but the intermediate range certainly displays the characteristics of Vinen turbulence, providing further proof that the normal turbulence observed at the plateau lacks significant flow structures larger than ℓ. This is in contrast to channel CF turbulence, where in the T II state, large-scale turbulence in both components develops due to interactions of the normal fluid with the channel walls, and the late decay $L(t) \propto t^{-3/2}$ is observed. It is fair to note that QT in spherical CF is inhomogeneous and anisotropic, requiring care in interpreting the experimental results. This is discussed in Ref. [5] as follows: Milliken *et al.* [41] showed that local decay of vorticity dominates over diffusive phenomena, and therefore the decay rate $dL/dt \propto -L^2$ first leads to homogenization of the vortex tangle. This occurs on the timescale of seconds for the estimated VLD profile in

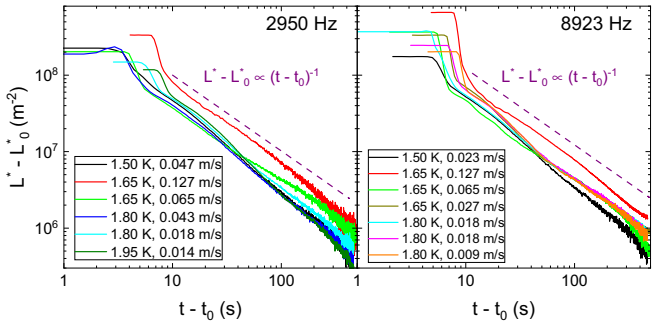

FIG. 3. Temporal decays $L^*(t)$ measured at the lower (≈2950 Hz, left) and higher (≈8920 Hz, right) resonance frequencies at various u_{ns} near the surface of the heater at bath temperatures as indicated, average of 50 decays. The dashed purple lines illustrate the inverse time decay. L_0^* is determined from late time values of vortex line density and varies between 10^4 and 10^5 m^{-2}; cf. also Fig. 2 in Ref. [5].

our experiment. Remaining vortices then decay as homogeneous Vinen turbulence, $L(t) \propto 1/t$, as observed.

We conclude that QT generated in spherical CF differs qualitatively from channel CF turbulence of He II and represents Vinen-type QT. Our data indicate that turbulence in the normal fluid is driven at small scales by a preexisting random tangle of quantized vortices, limiting its energy content and density, in stark contrast to channel CF, where shear flow leads to vortex line density enhancement. While the present phenomenology is incomplete, it captures the observed features of spherical CF within the range of investigated parameters. We believe that our results will stimulate further research needed for deeper understanding of this unique flow.

The authors acknowledge the help of E. Varga and stimulating discussions with S. Inui, K. R. Sreenivasan, and M. Tsubota. Support by the Czech Science Foundation (GAČR) under Project No. 20-00918S and by the Charles University Research program under Project No. START/SCI/053 is greatly appreciated.

[1] J. J. Niemela, L. Skrbek, K. R. Sreenivasan, and R. J. Donnelly, Turbulent convection at very high Rayleigh numbers, Nature (London) **404**, 837 (2000).

[2] J. T. Tough, *Superfluid Turbulence*, Progress in Low Temperature Physics Vol. VIII (North-Holland, Amsterdam, 1982).

[3] W. F. Vinen and J. J. Niemela, Quantum turbulence, J. Low Temp. Phys. **128**, 167 (2002).

[4] C. F. Barenghi, L. Skrbek, and K. R. Sreenivasan, Introduction to quantum turbulence, Proc. Natl. Acad. Sci. USA **111**, 4649 (2014).

[5] L. Skrbek, D. Schmoranzer, Š. Midlik, and K. R. Sreenivasan, Phenomenology of quantum turbulence in superfluid helium, Proc. Natl. Acad. Sci. USA **118**, e2018406118 (2021).

[6] W. F. Vinen, Mutual friction in a heat current in liquid helium II, I. Experiments on steady heat currents, Proc. R. Soc. A **240**, 114 (1957); II. Experiments on transient effects, *ibid.* **240**, 128 (1957); III. Theory of the mutual friction, *ibid.* **242**, 493 (1957); IV. Critical heat currents in wide channels, *ibid.* **243**, 400 (1958).

[7] E. Varga, Peculiarities of spherically symmetric counterflow, J. Low Temp. Phys. **196**, 28 (2019).

[8] S. Inui and M. Tsubota, Spherically symmetric formation of localized vortex tangle around a heat source in superfluid ^{4}He, Phys. Rev. B **101**, 214511 (2020).

[9] J. Schumacher and K. R. Sreenivasan, Colloquium: Unusual dynamics of convection in the Sun, Rev. Mod. Phys. **92**, 041001 (2020).
[10] G. Greenstein, Superfluid turbulence in neutron stars, Nature (London) **227**, 791 (1970).
[11] N. Andersson, T. Sidery, and G. L. Comer, Superfluid neutron star turbulence, Mon. Not. R. Astron. Soc. **381**, 747 (2007).
[12] R. Agrusta, J. van Hunen, and S. Goes, Strong plates enhance mantle mixing in early Earth, Nat. Commun. **9**, 2708 (2018).
[13] G. E. Volovik, *The Universe in a Helium Droplet* (Oxford University Press, Oxford, 2007).
[14] T. W. B. Kibble, Topology of cosmic domains and strings, J. Phys. A **9**, 1387 (1976).
[15] W. H. Zurek, Cosmological experiments in superfluid helium? Nature (London) **317**, 505 (1985).
[16] S. T. H. Hartman, H. A. Winther, and D. F. Mota, Collapse of spherical overdensities in superfluid models of dark matter, Astron. Astrophys. **639**, A90 (2020).
[17] R. J. Donnelly, *Quantized Vortices in Helium II* (Cambridge University Press, Cambridge, 1991).
[18] Except for remnant vortices, which in practice are almost always present in macroscopic samples of He II [19]; they might have been left from an earlier experiment, or might have been formed by the Kibble-Zurek mechanism [15] when cooled through the superfluid λ transition.
[19] D. D. Awschalom and K. W. Schwarz, Observation of a Remanent Vortex-Line Density in Superfluid Helium, Phys. Rev. Lett. **52**, 49 (1984).
[20] K. W. Schwarz, Three-dimensional vortex dynamics in superfluid ^{4}He: Homogeneous superfluid turbulence, Phys. Rev. B **38**, 2398 (1988).
[21] We emphasize that these two distinctly different regimes exist in the zero temperature regime with a possible cross-over between them [5].
[22] A. Marakov, J. Gao, W. Guo, S. W. Van Sciver, G. G. Ihas, D. N. McKinsey, and W. F. Vinen, Visualization of the normal-fluid turbulence in counterflowing superfluid ^{4}He, Phys. Rev. B **91**, 094503 (2015).
[23] S. Yui and M. Tsubota, Counterflow quantum turbulence of He-II in a square channel: Numerical analysis with nonuniform flows of the normal fluid, Phys. Rev. B **91**, 184504 (2015).
[24] J. Gao, W. Guo, V. S. L'vov, A. Pomyalov, L. Skrbek, E. Varga, and W. F. Vinen, Decay of counuterflow turbulence in superfluid ^{4}He, JETP Lett. **103**, 648 (2016).
[25] S. Babuin, V. S. L'vov, A. Pomyalov, L. Skrbek, and E. Varga, Coexistence and interplay of quantum and classical turbulence in superfluid ^{4}He: Decay, velocity decoupling, and counterflow energy spectra, Phys. Rev. B **94**, 174504 (2016).
[26] D. J. Melotte and C. F. Barenghi, Transition to normal fluid turbulence in helium II, Phys. Rev. Lett. **80**, 4181 (1998).
[27] W. Guo, S. B. Cahn, J. A. Nikkel, W. F. Vinen, and D. N. McKinsey, Visualization study of counterflow in superfluid ^{4}He using metastable helium molecules, Phys. Rev. Lett. **105**, 045301 (2010).
[28] E. Rickinson, C. F. Barenghi, Y. A. Sergeev, and A. W. Baggaley, Superfluid turbulence driven by cylindrically symmetric thermal counterflow, Phys. Rev. B **101**, 134519 (2020).
[29] Y. A. Sergeev and C. F. Barenghi, Turbulent radial thermal counterflow in the framework of the HVBK model, Europhys. Lett. **128**, 26001 (2019).
[30] See Supplemental Material at http://link.aps.org/supplemental/10.1103/PhysRevFluids.9.L022601 for together with Refs. [42–52] cited therein for details on the spatial temperature profile calculations/measurements and on the numerical methods employed.
[31] Z. Xie, Y. Huang, F. Novotný, S. Midlik, D. Schmoranzer, and L. Skrbek, Spherical thermal counterflow of He II, J. Low Temp. Phys. **208**, 426 (2022).
[32] E. Varga and L. Skrbek, Thermal counterflow of superfluid ^{4}He: Temperature gradient in the bulk and in the vicinity of the heater, Phys. Rev. B **100**, 054518 (2019).
[33] E. Varga, M. J. Jackson, D. Schmoranzer, and L. Skrbek, The use of second sound in investigations of quantum turbulence in He II, J. Low Temp. Phys. **197**, 130 (2019).
[34] R. J. Donnelly and C. F. Barenghi, The observed properties of liquid helium at the saturated vapor pressure, J. Phys. Chem. Ref. Data **27**, 1217 (1998).
[35] D. D. Holm, Introduction to HVBK dynamics, in *Quantized Vortex Dynamics and Superfluid Turbulence*, edited by C. F. Barenghi, R. J. Donnelly, and W. F. Vinen (Springer, Berlin, 2001), pp. 114–130.

[36] E. Varga, S. Babuin, and L. Skrbek, Second-sound studies of coflow and counterflow of superfluid ^{4}He in channels, Phys. Fluids **27**, 065101 (2015).
[37] D. Schmoranzer, M. J. Jackson, Š. Midlik, M. Skyba, J. Bahyl, T. Skokánková, V. Tsepelin, and L. Skrbek, Dynamical similarity and instabilities in high Stokes number oscillatory flows of superfluid helium, Phys. Rev. B **99**, 054511 (2019).
[38] G. Swaminathan, K. Chandra Sahu, A. Sameen, and R. Govindarajan, Global instabilities in diverging channel flows, Theor. Comput. Fluid Dyn. **25**, 53 (2011).
[39] V. Shtern and F. Hussain, Effect of deceleration on jet instability, J. Fluid Mech. **480**, 283 (2003).
[40] P. J. Morris, The spatial viscous instability of axisymmetric jets, J. Fluid Mech. **77**, 511 (1976).
[41] F. Milliken, K. Schwarz, and C. Smith, Free decay of superfluid turbulence, Phys. Rev. Lett. **48**, 1204 (1982).
[42] S. Babuin, M. Stammeier, E. Varga, M. Rotter, and L. Skrbek, Quantum turbulence of bellows-driven ^{4}He superflow: Steady state, Phys. Rev. B **86**, 134515 (2012).
[43] R. A. Ashton, L. B. Opatowsky, and J. T. Tough, Turbulence in pure superfluid flow, Phys. Rev. Lett. **46**, 658 (1981).
[44] T. V. Chagovets and L. Skrbek, Steady and decaying flow of He II in a channel with ends blocked by superleaks, Phys. Rev. Lett. **100**, 215302 (2008).
[45] K. P. Martin and J. T. Tough, Evolution of superfluid turbulence in thermal counterflow, Phys. Rev. B **27**, 2788 (1983).
[46] R. K. Childers and T. Tough, Helium II thermal counterflow: Temperature- and pressure-difference data and analysis in terms of the Vinen theory, Phys. Rev. B **13**, 1040 (1976).
[47] G. A. Glatzmaier, Numerical simulations of stellar convective dynamos. I. The model and method, J. Comput. Phys. **55**, 461 (1984).
[48] U. R. Christensen and J. Wicht, Numerical dynamo simulations, in *Treatise on Geophysics*, edited by G. Schubert (Elsevier, 2015), pp. 245–277.
[49] K. M. Soderlund, B. E. Schmidt, J. Wicht, and D. D. Blankenship, Ocean-driven heating of europa's icy shell at low latitudes, Nature Geosci, **7**, 16 (2014).
[50] J. Kvorka and O. Čadek, A numerical model of convective heat transfer in Titan's subsurface ocean, Icarus **376**, 114853 (2022).
[51] V. K. Khersonskii, D. A. Varshalovich, A. N. Moskalev, *Quantum Theory of Angular Momentum* (World Scientific, 1988).
[52] C. Dumoulin, O. Čadek, and G. Choblet, Predicting surface dynamic topographies of stagnant lid planetary bodies, Geophys. J. Intl. **195**, 1494 (2013).